J Therm Anal Calorim (2013) 114:549–555
DOI 10.1007/s10973-013-3001-y

Preparation and characterization of the bacterial cellulose/polyurethane nanocomposites

Elaine R. P. Pinto · Hernane S. Barud · Wagner Luiz Polito · Sidney J. L. Ribeiro · Younès Messaddeq

Received: 22 October 2012 / Accepted: 18 January 2013 / Published online: 12 February 2013

Abstract New nanocomposites based on bacterial cellulose nanofibers (BCN) and polyurethane (PU) prepolymer were prepared and characterized by SEM, FT-IR, XRD, and TG/DTG analyses. An improvement of the interface reaction between the BCN and the PU prepolymer was obtained by a solvent exchange process. FT-IR results showed the main urethane band at 2,270 cm^{-1} to PU prepolymer; however, in nanocomposites new bands appear as disubstituted urea at 1,650 and 1,550 cm^{-1}. In addition, the observed decrease in the intensity of the hydroxyl band (3,500 cm^{-1}) suggests an interaction between BCN hydroxyls and NCO-free groups. The nanocomposites presented a non-crystalline character, significant thermal stability (up to 230 °C) and low water absorption when compared to pristine BCN.

Keywords Bacterial cellulose nanofibers · Polyurethane prepolymer · Nanocomposites

Introduction

The development of new composite materials from nanofibers and polymers of different classes have aroused a great technological interest because they have improved characteristics, such as flexibility, low density, hardness among others. A special class of composites includes nanocomposites, where aspects such as biodegradability must be considered [1, 2].

Bacterial cellulose nanofibers (BCN) are interesting materials to produce the new composites. BCN are produced in static culture medium by bacteria of the genus *Gluconacetobacter xylinuns* obtained in the form of highly hydrated hydrogels in a 3D nanofibers network (nanocellulose) [3]. Relevant features compared to plant cellulose fibers include higher crystallinity, tensile strength, elasticity, durability, and absorption capacity [4–6]. Cellulose fibers present free hydroxyl functional groups that are involved intra- and intermolecular hydrogen bonds, important feature in the preparation of different composite materials. Owing to these important properties, BCN has been used for the preparation of a great number of new composites including antimicrobial materials, optical composites, green composites, and ecocomposites [3, 7–10].

On the other hand, polyurethanes (PU) constitute an important class of polymers with several different properties and applications in industrial scale in areas such as biomedical, foams, coating, adhesives, fibers, composites, and elastomers [11]. In addition, PU materials are in general produced by chemical reaction between polyols and isocyanates functional groups. In particular, in this study, the castor oil is the main polyol used to synthesize PU prepolymer. Castor oil is obtained from seeds of the *Ricinus communis*, the interesting point concerning this natural oil is its composition, of around 90 % of the triglyceride of 12-hydroxyoleic acid, also known as ricinoleic acid. Moreover, in the field of biodegradable PU, the castor oil has been suggested as potentially interesting material [12–14].

Apart from BCN and PU prepolymer, two interesting materials, to produce the composites, they need a good

E. R. P. Pinto (✉) · H. S. Barud · S. J. L. Ribeiro · Y. Messaddeq
Chemistry Institute, São Paulo State University-UNESP, São Paulo, Brazil
e-mail: elainerpp@yahoo.com.br

W. L. Polito
Chemistry Institute, São Paulo University-USP, São Carlos, Brazil

interface adhesion between fiber and matrix. The interface improves the stress transfer from the matrix to fibers and thus improving the mechanical strength of the composites [2]. In addition, there are physical and chemical methods to improve the interfacial adhesion. Physical methods, including corona or plasma discharges, are useful for polymers such as polypropylene, polyethylene, and polystyrene [15]. Chemical methods, covering pretreatment of fibers surface with a coupling agent, such as silanes, isocyanates [16], and the modification of the matrix by grafting polar moieties, such as acrylic acid, acrylic esters, or maleic anhydride onto polymer chains [17, 18] are also being addressed.

Chemical reactions between PU resins and microcrystalline cellulose are being considered as reinforcement of the PU matrix. Wu et al. [19] dispersed microcrystalline cellulose in the PU prepolymer in order to obtain composites. Seydibeyoglu and Oksman [20] prepared the composites by compression molding, by stacking the cellulose fiber mats between PU films. New organic aerogels were prepared using cellulose derivatives as precursors. Gels were synthesized in acetone by cross linking cellulose acetate with a non-toxic isocyanate and a tin-based catalyst [21].

Although, there are several researches dedicated to BCN no there are studies reported regarding the interaction of BCN and PU prepolymer used from renewable sources. BCN/PU nanocomposites could be interesting to produce multifunctional bio-nanocomposites for several applications, include flexible substrate for OLED devices [3, 8, 22]. In order to produce BCN/PU nanocomposites with a good interface, this study submitted the hydrated BCN to a simple approach involving the exchange solvent process [23]. This approach is fundamental to improve the interaction between BCN and PU prepolymer. The BCN-PU nanocomposites were characterized by Scanning Electron Microscopy (SEM), Fourier Transform infrared spectroscopy (FT-IR), and X-rays diffraction (XRD). The thermal stability was evaluated by Thermogravimetry (TG/DTG) and swelling behavior has been also considered.

Experimental

Materials

The PU prepolymer was supplied by Terra Azul Ltda, Brazil Company. It is synthesized with 1,4-toluene-diisocyanate (TDI—80:20) and a polyol consisting of castor oil as main component. It presented 3 % of free-NCO groups [24].

BCN membranes were obtained from cultivation of the *Gluconacetobacter hansenii* strain ATCC 23769. Cultivation medium was conducted for 96 h at 28 °C in trays 30 cm × 50 cm, containing the sterile medium composed of glucose 50 g L^{-1}, yeast extracts 4 g L^{-1}, anhydrous disodium phosphate 2 g L^{-1}, heptahydrated magnesium, sulfate 0.8 g L^{-1}, and ethanol 20 g L^{-1}. After 96 h, hydrated BCN hydrogels (3-mm thick) containing up to 99 % of water and 1 % of cellulose were obtained. The membranes were several times washed in water and followed with 1 wt% aqueous NaOH at 70 °C in order to remove the bacteria until neutral pH.

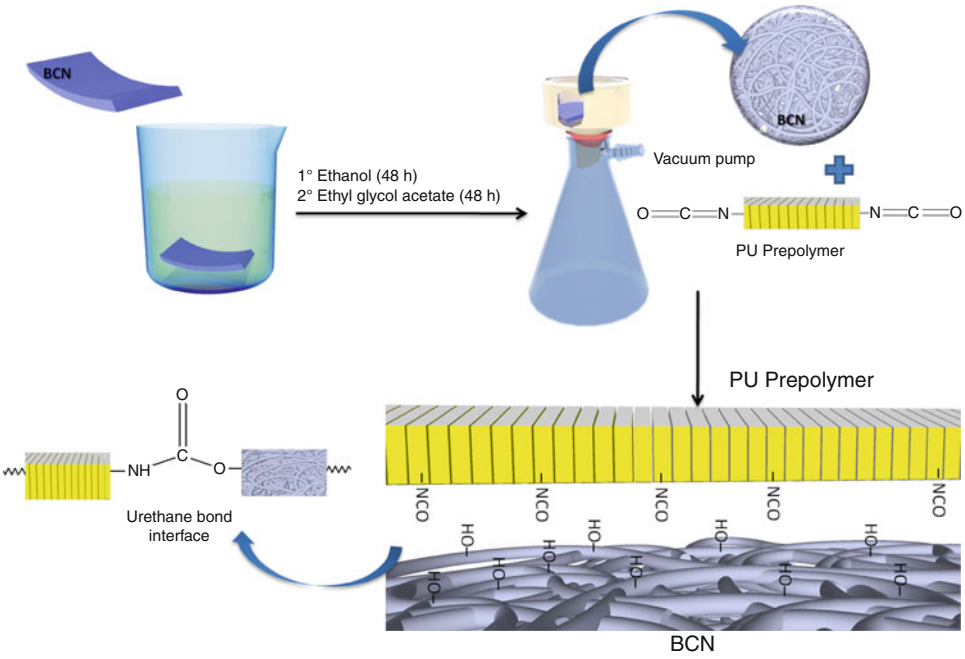

Fig. 1 Representative process of the interface adhesion reaction between BCN and PU prepolymer

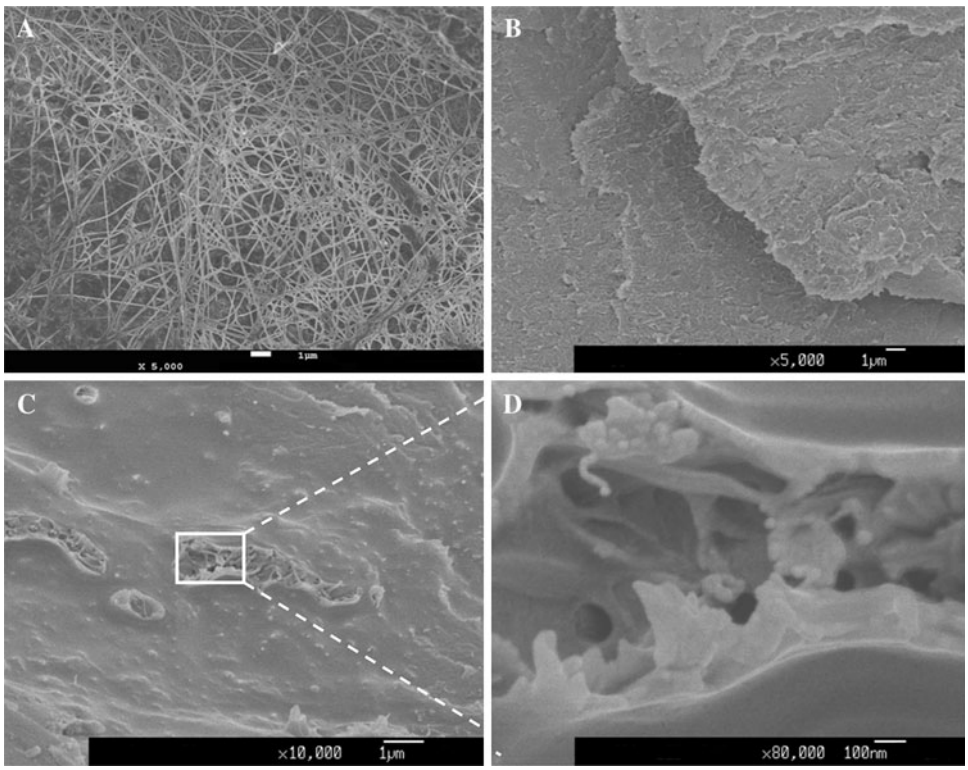

Fig. 2 SEM images of: **a** Freeze-dried BCN membrane surface; **b** BCN/PU 1 nanocomposite surface; **c** surface image detail of BCN/PU 1 nanocomposite (*low magnification*) and **d** detail of BCN/PU 1 nanocomposite (*high magnification*)

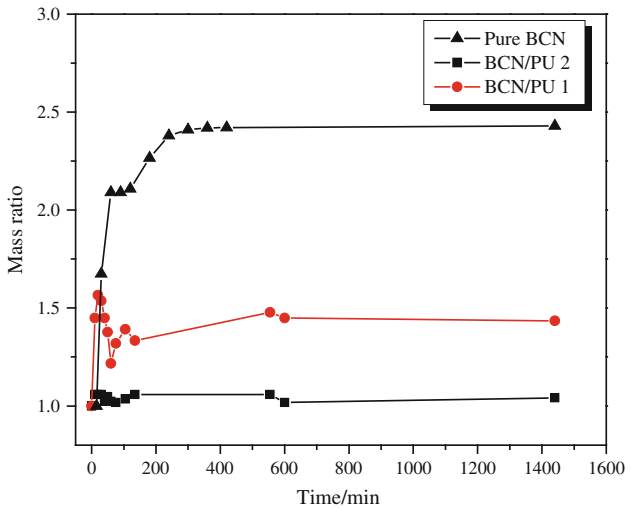

Fig. 3 Swelling ability among nanocomposites (BCN/PU 1 and BCN/PU 2) and pure BCN

Preparation of the composites

The hydrated BCN membranes were submitted to a solvent exchange process for 48-h soaking in ethanol and further 48 h in ethyl glycol acetate. After this period, swollen ethyl glycol acetate the BCN membranes were utilized for the nanocomposite preparation. The BCN membranes were cut 5 cm × 5 cm pieces and the samples of masses were measures. A Buchner filtering system was used to improve the penetration of PU prepolymer into membranes. The nanocomposites (BCN/PU) were prepared in the mass proportion 1:1 (BCN/PU 1) and 1:2 (BCN/PU 2) to analyze the influence of the prepolymer in interface nanocomposites.

Characterization of the composites

Scanning electron microscopy (SEM) study was performed in FEG-SEM JSM 6330F microscope. The nanocomposites were coated with a 3-nm thick carbon layer.

X-ray diffraction (XRD) patterns were recorded using a Siemens Kristalloflex X-ray diffractometer at room temperature using nickel filtered Cu Kα radiation. Patterns were recorded from 4° to 70° (2θ angle), steps of 0.02° and a step time of 3 s.

The FT-IR analyses were carried out using a Perkin-Elmer 2000 spectrometer. Infrared transmission spectra were obtained from 4,000 to 400 cm^{-1}. Each sample was scanned 32 times at a resolution of 4 cm^{-1} and the scans were signal averaged. Potassium bromide (KBr) pellets method was used with the proportion 1:100 of the sample and KBr. The samples were milled with KBr to form a very fine powder. This powder is then compressed into thin pellets which were analyzed.

Thermogravimetric analyze (TG) measurements were carried out using a TA Instruments SDT 600 under dynamical nitrogen atmosphere with a flow rate of 100 mL min^{-1} and a heating rate of 10 °C min^{-1} in the range of 20–600 °C. All samples had approximately 10 mg.

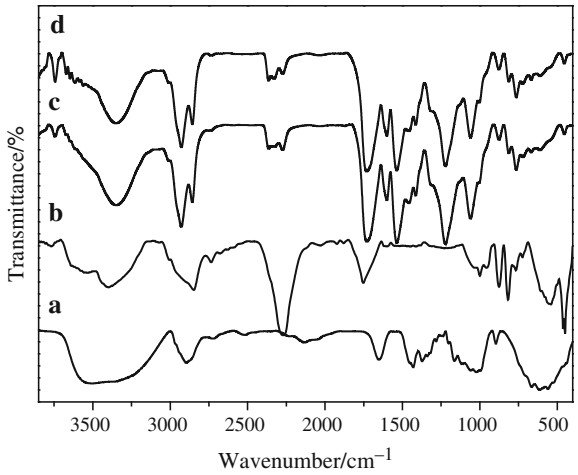

Fig. 4 FT-IR spectra of: *a* Pure BCN; *b* PU prepolymer film; *c* BCN/PU 1 nanocomposite and *d* BCN/PU 2 nanocomposite

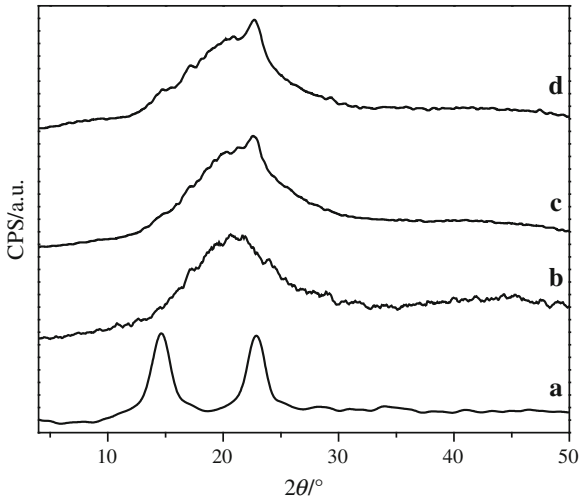

Fig. 5 Diffraction patterns obtained for: *a* Dried BCN; *b* PU prepolymer; *c* BCN/PU 1 nanocomposite and *d* BCN/PU 2 nanocomposite

Water swelling was evaluated with dried membranes, cut into disk shapes with 0.6-in diameter, and the samples of masses were measures. Samples were immersed in deionized water for different times up to 24 h at room temperature. Swelling was calculated as follows:

$$\text{Swelling} = \frac{(G_{s,t}) - (G_i)}{G_i}$$

where G_i is the initial mass of dried sample and $G_{s,t}$ is the mass of samples in swollen state.

Results and discussion

The nanocomposites BCN/PU were produced and the solvent exchange had a fundamental importance in the preparation of this nanocomposites. Notably, BCN/PU nanocomposites have the interface formed from urethane bond, which it was as result of the reaction between –OH groups from BCN and free –NCO groups in PU prepolymer. However, other reactions may have occurred due to the residual water presence on never-dried BCN membranes could be reacting with PU prepolymer leading to CO_2 release and, consequently, appearance of bubbles [7, 11]. This fact is not desirable, and to eliminate this problem and promote a good interface interaction between BCN and PU prepolymer, we proposed an exchange solvent process in the nanocomposite preparation. This way, to decrease this unwanted effect, the literature results have demonstrated the influence of solvent exchange process for cellulose and derivatives [25] and other fibers [26] to improve the interaction between fiber and polymeric matrix.

Never-dried BCN were soaked in ethanol followed by ethyl glycol acetate. But, the BCN has strong interactions between water and ethanol; however, these solvents are reactive toward PU prepolymer. Alternatively, the ethyl glycol acetate was chosen with the goal to improve the interface interactions between BCN and PU prepolymer and, to remove the water and ethanol excesses. All BCN/PU samples were produced from incorporation of the PU prepolymer by vacuum Buchner filtering system. Vacuum process was efficient to increase the PU prepolymer penetration into BCN network and final curing process was carried out by air moisture and solvent casting, Fig. 1.

The formation of the BCN/PU nanocomposites includes a combination of the reactions between hydroxyl groups (–OH) from BCN with –free-NCO from PU prepolymer to produce the urethane groups. Other secondary reaction could occur with residual water and ethanol molecules present in BCN bulk [27], in this case the reaction produce urea bonds. The representative process to produce the BCN/PU nanocomposite is shown in Fig. 1 with the urethane bond as main group obtained in interface.

Figure 2 shows SEM images for freeze-dried BCN and representative BCN/PU 1 nanocomposite. Figure 1a reveals that freeze dried BCN is formed by porous 3D network structure formed by long cellulose nanofibers [23]. Figure 1b shows surface image of the BCN/PU 1 nanocomposite, where BCN surface appears totally covered by PU prepolymer. Figures 1c, d show in more details of the PU prepolymer filled BCN pores. In addition, bacterial cellulose nanofibrils appear well integrated within PU prepolymer, indicating a good interface adhesion between the BCN and PU prepolymer.

The swelling behavior of the BCN/PU nanocomposites reveals a diminishing in the water absorption (Fig. 3). These results evidenced that the PU prepolymer covered

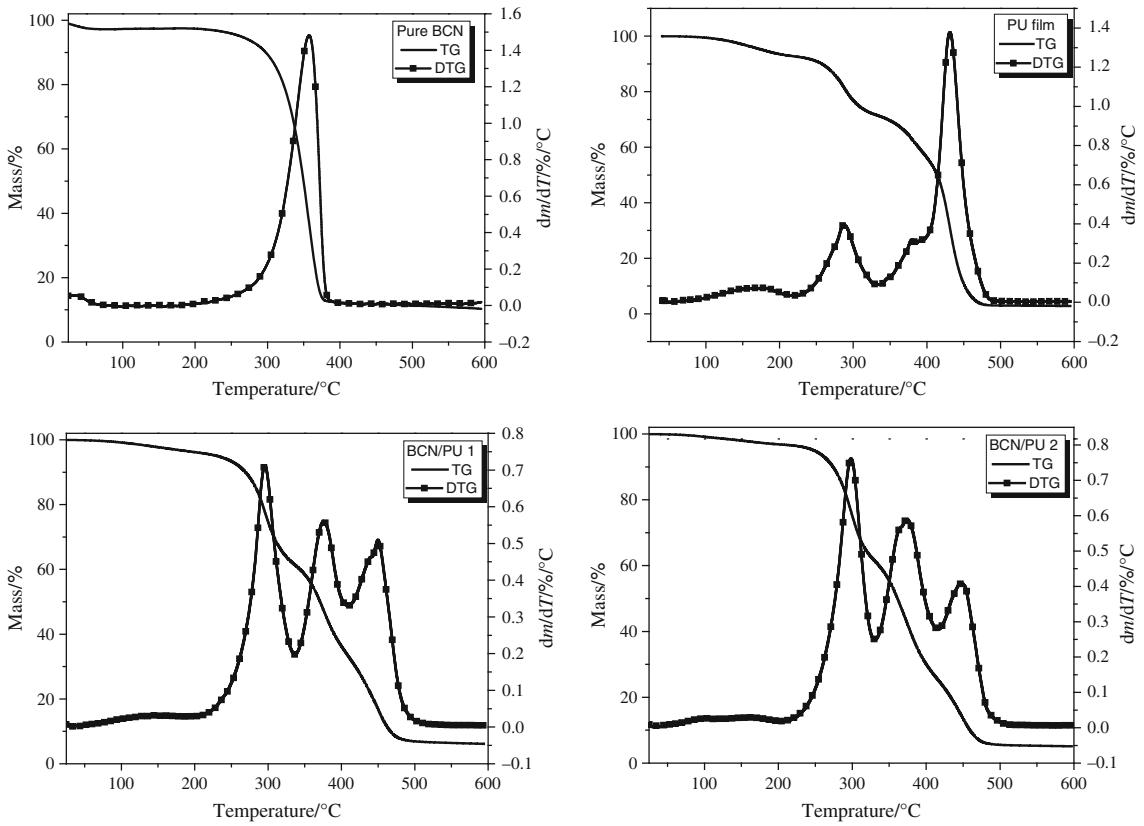

Fig. 6 TG and DTG curves: pure BCN; PU film; nanocomposites BCN/PU 1 and BCN/PU 2

Table 1 Results from TG and DTG curves of the pure BCN, PU film, and nanocomposites

Samples	Mass loss/% at 200 °C	Temperatures/°C					Residues/%
		T *onset*	T *endset*	1° peak DTG	2° peak DTG	3° peak DTG	
Pure BCN	2.7	310.4	369.9	350.8	–	–	20.6
PU film	6.5	264.9	456.5	286.3	378.1	430.2	2.9
BCN/PU 1	3.6	265.7	469.5	298.2	373.5	450.5	5.3
BCN/PU 2	2.9	271.8	469.4	296.0	374.9	450.2	6.4

the BCN surface and also penetrated on pores blocking the entrance of water, as showed before by SEM images.

The main absorption occurs after 1 h and remains constant for all nanocomposites. For BCN membrane an increasing behavior is observed within the initial 2 h stabilizing after 6 h. This behavior must be due to both chemical and physical structure; BCN is in fact hydrophilic and strong water absorption is expected; concerning the physical structure, BCN is three-dimensional non-woven network with large amount of pores which is expected to generate the capillary forces contributing to water sorption [1, 28, 29].

The nanocomposites presented different behaviors in swelling results. The BCN/PU 1 presented a swelling of the 60 %, while the BCN/PU 2 only 40 % of the swelling. The results indicated that the nanocomposite BCN/PU 2 blocked the water more efficiently than BCN/PU 1, probably due to more PU prepolymer content in BCN/PU 2. Therefore, PU prepolymer could be an important key to control the water absorption in cellulose nanocomposites.

FT-IR spectroscopy (Fig. 4) was used to investigate the structural difference in BCN, PU prepolymer and nanocomposites synthesized. The mains bands observed for pure BCN (Fig. 4a) are assigned to OH stretching (3,450 cm^{-1}), H-bonds (3,250 cm^{-1}), CH stretching of CH_2 and CH_3 groups (2,900–2,700 cm^{-1}), CH_2 symmetric bending (1,430 cm^{-1}), CH bending (1,370 cm^{-1}), anti-symmetric bridge C–O–C stretching (1,160 cm^{-1}), skeletal

vibrations involving C–O stretching (1,114–1,060 cm^{-1}), antisymmetric out-of-phase stretching (896 cm^{-1}), and OH out-of-phase bending (666–619 cm^{-1}) [7, 30, 31]. To PU prepolymer spectrum (Fig. 4b) bands are assigned to urethane linkages at 3,500–3,300 cm^{-1} (N–H), and according to Coleman [32] the peak that corresponds to N–H–O–C=O hydrogen-bonding appears as shoulder at about 3,255–3,265 and 2,270 cm^{-1} free-NCO group, 1,730 cm^{-1} are assigned to carbonyl, methyl groups at 2,960 cm^{-1} and C–O 1,100 cm^{-1} of the polyol.

The spectra obtained for nanocomposites (Fig. 4c, d) shows bands that are identified in pure BCN and PU prepolymer. In addition, new peaks appear at 1,650 and 1,550 cm^{-1} (N–H, CO–NH) due the reaction between swollen BCN membranes and PU prepolymer. However, the FT-IR spectra quantitative analysis was not suitable, but the decreasing of the relative intensity of free-NCO (2,270 cm^{-1}) peak in the nanocomposite when compared with the spectrum obtained for pure PU prepolymer also suggest that the reaction occurred. Other peaks are observed indicating secondary reactions, e.g., a peak at 1,640 cm^{-1}, typical of allophanates, and peaks around 1,450 cm^{-1} of isocyanurate resulting from reactions between isocyanate and urethane groups [33].

Figure 5 shows XRD patterns for all samples. Broad diffraction peaks are observed at 15° and 22.6° for the pure BCN membrane (Fig. 5a), characteristics of cellulose I_α and I_β phases ($100_{1\alpha}$, $110_{1\beta}$, and $010_{1\beta}$ planes at 15° and $110_{1\alpha}$ and $200_{1\beta}$ at 22.5°) [34, 35]. A broad diffraction peak at 21° is observed in the diffraction pattern of PU prepolymer film (Fig. 5b), confirming the amorphous character usually observed for aromatic isocyanate PU [36].

X-ray diffraction patterns observed for BCN/PU nanocomposites (Fig. 5c, d) present the convolution of the broad PU component peaking at 21° and the cellulose peak at 22.6°. Interesting enough, the cellulose peak at 15° is not observed with the same relative intensity for the nanocomposites. On the other hand, these results provide additional evidence that the original crystalline structure of cellulose (cellulose I) is still in the nanocomposite [19].

Thermal stability was evaluated by TG/DTG curves presented in Fig. 6. The TG curve obtained for pure BCN shows two events of mass loss. The first event involving 2.7 % mass loss occurs continuously from 25 to 250 °C due to water and solvent loss. The second loss is observed in the temperature range from 250 to 380 °C, attributed to BCN pyrolysis [37]. DTG curve shows maximum decomposition at 351 °C. Table 1 presents the main temperatures and mass loss from TG and DGT curves to all samples.

The TG curve obtained for PU film shows four important steps. The major breakdown PU products from thermal degradation were studied by Javni [38, 39] three mechanisms of decomposition of urethane bonds have already been proposed. DTG curve presents the first event, it refers to solvent evaporation, involving 7 % of mass loss and occurring from room temperature up to 240 °C. Subsequently, PU film decomposition occurs in more three steps, which can also be seen in the DTG curve. In the first one the highest temperature is near to 286 °C, the next peak occurred an overlap at 378.1 and 430 °C.

The shapes of the mass loss curves observed for nanocomposites are almost identical and overall differences in thermal stability seen to be small. T *onset* increase to nanocomposites (266 and 272 °C), when compared to pristine PU film. This increase is corroborated as proposed model for the process of the interface adhesion reaction between two polymers, Fig. 1, and also suggested by SEM images, Fig. 2.

Degradation processes of BCN/PU nanocomposites presented three steps, which can see in DTG curves, so the maxima temperature at 298, 375, and 450 °C. Residues are observed due to the nitrogen atmosphere used in the measurements (Table 1); however, there were significant differences in residues. The nanocomposites residues presented fewer residues than BCN and more than PU film, these results suggest that PU film made a good interface and this interaction contributed to decomposition of the surface that was covered with PU film.

Conclusions

Nanocomposite membranes based on BCN and PU prepolymer have been obtained by a solvent exchange method to improve BCN and PU surface interface interactions. SEM images show an effective coating of the BCN by PU prepolymer and also suggest a good interface adhesion between two polymers. According to swelling measurements, the PU contents could be an important key to control the water absorption in cellulose nanocomposites. BCN/PU nanocomposites present higher thermal stability when compared to pristine PU film. Potential applications in electronic devices of these nanocomposites membranes have been studied.

Acknowledgements Financial support from Brazilian agencies "Fundação de amparo a pesquisa do estado de São Paulo (FAPESP), Coordenação de Aperfeiçoamento de Pessoal de Nível Superior (CAPES)" and "Conselho Nacional de Desenvolvimento Científico e Tecnológico (CNPq)" and technical support from Electron Microscopy Laboratory/National Synchrotron Light Laboratory (LME/LNLS) are acknowledged.

References

1. Czaja WK, Young DJ, Kawecki M, Brown RM. The future prospects of microbial cellulose in biomedical applications. Biomacromolecules. 2007;8:1–12.

2. Matthews FL, Rawlings RD. Composite materials: engineering and science. London: Chapman & Hall; 1994.
3. Yano H, Sugiyama J, Nakagaito AN, Nogi M, et al. Optically transparent composites reinforced with networks of bacterial nanofibers. Adv Mater. 2005;17:153–5.
4. Gatenholm P, Klemm D. Bacterial nanocellulose as a renewable material for biomedical applications. MRS Bull. 2010;35:208–13.
5. Klemm D, Schumann D, Udhardt U, Marsch S. Bacterial synthesized cellulose-artificial blood vessels for microsurgery. Prog Polym Sci. 2001;26:1561–603.
6. Klemm D, Heublein B, Fink HP, Bohn A. Cellulose: fascinating biopolymer and sustainable raw material. Angew Chem Int Edit. 2005;44:3358–93.
7. Pinto ERP. Estudo do sistema Celulose Bacteriana-Poliuretano para a produção de novos compósitos. Master Science Dissertation. Universidade Estadual Paulista, Instituto de Química, Brazil. 2007;1–170.
8. Nogi M, Yano H. Transparent nanocomposites based on cellulose produced by bacteria offer potential innovation in the electronics device industry. Adv Mater. 2008;20:1849–52.
9. Hu L, Wan YZ, He F, Luo HL, et al. Effect of coupling treatment on mechanical properties of bacterial cellulose nanofibre-reinforced UPR ecocomposites. Mater Lett. 2009;63:1952–4.
10. Maria LCS, Santos ALC, Oliveira PC, Valle ASS, et al. Preparation and antibacterial activity of silver nanoparticles impregnated in bacterial cellulose. Polimeros. 2010;20:72–7.
11. Vilar W. Química e Tecnologia dos poliuretanos. Rio de Janeiro: Vilar Consultoria; 2004.
12. Ionescu M, Sinharoy S, Petrovic ZS. Polyacetal polyols for polyurethanes. J Polym Environ. 2009;17:123–30.
13. Palaskar DV, Boyer A, Cloutet E, Alfos C, Cramail H. Synthesis of biobased polyurethane from oleic and ricinoleic acids as the renewable resources via the AB-type self-condensation approach. Biomacromolecules. 2010;11:1202–11.
14. Petrovic ZS, Cvetkovic I, Hong D, Wan XM, et al. Vegetable oil-based triols from hydroformylated fatty acids and polyurethane elastomers. Eur J Lipid Sci Technol. 2010;112:97–102.
15. Bledzki AK, Gassan J. Composites reinforced with cellulose based fibres. Prog Polym Sci. 1999;24:221–74.
16. Qiu WL, Zhang FR, Endo T, Hirotsu T. Isocyanate as a compatibilizing agent on the properties of highly crystalline cellulose/polypropylene composites. J Mater Sci. 2005;40:3607–14.
17. Botaro VR, Gandini A, Belgacem MN. Heterogeneous chemical modification of cellulose for composite materials. J Thermoplast Compos Mater. 2005;18:107–17.
18. Qiu WL, Endo T, Hirotsu T. Interfacial interactions of a novel mechanochemical composite of cellulose with maleated polypropylene. J Appl Polym Sci. 2004;94:1326–35.
19. Wu QJ, Henriksson M, Liu X, Berglund LA. A high strength nanocomposite based on microcrystalline cellulose and polyurethane. Biomacromolecules. 2007;8:3687–92.
20. Seydibeyoglu MO, Oksman K. Novel nanocomposites based on polyurethane and micro fibrillated cellulose. Compos Sci Technol. 2008;68:908–14.
21. Fischer F, Rigacci A, Pirard R, Berthon-Fabry S, Achard P. Cellulose-based aerogels. Polymer. 2006;47:7636–45.
22. Nakagaito AN, Nogi M, Yano H. Displays from transparent film of natural nanofibers. MRS Bull. 2010;35:214–8.
23. Barud HS, Souza JL, Santos DB, Crespi MS, Ribeiro CA, Messaddeq Y, Ribeiro SJL. Bacterial cellulose/poly(3-hydroxybutyrate) composite membranes. Carbohydr Polym. 2011;83:1279–84.
24. ASTM. D2572–03: standard test method for isocyanate groups in urethane materials or prepolymers. West Conshohocken: Pennsylvania; 2003.
25. Mantanis GI, Young RA, Rowell RM. Swelling of compressed cellulose fiber webs in organic liquids. Cellulose. 1995;2:1–22.
26. Kunzek H, Muller S, Vetter S, Godeck R. The significance of physico chemical properties of plant cell wall materials for the development of innovative food products. Eur Food Res Technol. 2002;214:361–76.
27. Lee KY, Bismarck A. Susceptibility of never-dried and freeze-dried bacterial cellulose towards esterification with organic acid. Cellulose. 2012;19:891–900.
28. Jonoobi M, Harun J, Mathew AP, Hussein MZB, Oksman K. Preparation of cellulose nanofibers with hydrophobic surface characteristics. Cellulose. 2010;17:299–307.
29. Matsuda T, Kurohane K, Imai Y. Di-(2-ethylhexyl) phthalate enhances skin sensitization to isocyanate haptens in mice. Toxicol Lett. 2010;192:97–100.
30. Barud HS, de Araujo AM, Santos DB, de Assuncao RMN, et al. Thermal behavior of cellulose acetate produced from homogeneous acetylation of bacterial cellulose. Thermochim Acta. 2008;471:61–9.
31. Silverstein RM, Bassler GC, Morrill TC. Identificação espectrométrica de compostos orgânicos. Rio de Janeiro: LTC; 1994.
32. Coleman MM, Lee KH, Skrovanek DJ, Painter PC. Hydrogen-bonding in polymers. 4. Infrared temperature studies of a simple polyurethane. Macromolecules. 1986;19:2149–57.
33. Rivera-Armenta JL, Heinze T, Mendoza-Martinez AM. New polyurethane foams modified with cellulose derivatives. Eur Polym J. 2004;40:2803–12.
34. Osullivan AC. Cellulose: the structure slowly unravels. Cellulose. 1997;4:173–207.
35. Wada M, Okano T. Localization of I-alpha and I-beta phases in algal cellulose revealed by acid treatments. Cellulose. 2001;8:183–8.
36. Cao Q, Liu PS. Structure and mechanical properties of shape memory polyurethane based on hyperbranched polyesters. Polym Bull. 2006;57:889–99.
37. Barud HS, Ribeiro CA, Crespi MS, Martines MAU, et al. Thermal characterization of bacterial cellulose-phosphate composite membranes. J Therm Anal Calorim. 2007;87:815–8.
38. Husic S, Javni I, Petrovic ZS. Thermal and mechanical properties of glass reinforced soy-based polyurethane composites. Compos Sci Technol. 2005;65:19–25.
39. Javni I, Petrovic ZS, Guo A, Fuller R. Thermal stability of polyurethanes based on vegetable oils. J Appl Polym Sci. 2000;77:1723–34.